# Journal of Materials Chemistry A

Accepted Manuscript


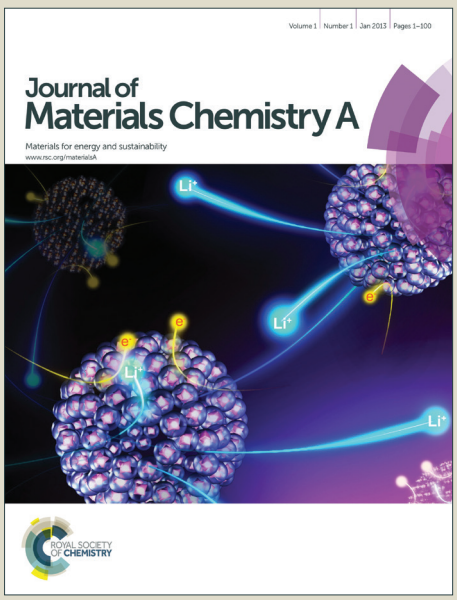





ROYAL SOCIETY OF CHEMISTRY

www.rsc.org/materialsA

RSCPublishing

COMMUNICATION

# $TiO_2$ mesocrystals built of nanocrystals with exposed {001} facets: Facile synthesis and superior photocatalytic ability

Cite this: DOI: 10.1039/x0xx00000x

Received 00th January 2012,
Accepted 00th January 2012

DOI: 10.1039/x0xx00000x

www.rsc.org/

Yanna Guo,[a] Hui Li,[a] Jin Chen,[a] Xuejing Wu[a] and Lei Zhou*[ab]

**In this work, a totally novel, extremely easy, much greener and low-cost method has been developed to synthesize $TiO_2$ mesocrystals. These materials are built of $TiO_2$ nanocrystals with similar crystallographic orientation and largely exposed {001} facets. Their unique structure optimizes the relationship between specific surface area, crystallite size and highly active facets, and therefore leads to a superior photocatalytic activity.**

Internal structure and external shape of a material are very important to its properties. In order to get high performance materials, the structure and shape have to be carefully optimized or designed. Taking widely-used $TiO_2$ materials as examples, large crystallite size (means structure coherence and helpful to electron-hole separation), large specific surface area (means more reaction sites) and large exposure of highly active facets (means high reaction activity on the reaction sites) are all necessary for us to get a high photocatalytic ability.[1-3] However, it is hard for a structure model to satisfy all these three requirements, because to some extent these requirements are contradictive. A few common structure models of $TiO_2$ materials with exposed {001} facets are shown in Fig. 1. *a) Micro-sized single crystals.*[4-7] These materials have relatively large sizes and are highly crystallized. However the large sizes usually put bounds to their specific surface areas. *b) Nanocrystals.*[8-12] Their small sizes usually lead to large specific surface area. However a smaller crystallite size may also facilitate the electron-hole recombination and therefore offsets the benefits from the large surface area. Another issue is that nanocrystals are difficult to be removed from the system and not suitable for practical applications. *c) Porous single crystal.*[13-15] These materials promise a good structure coherence and large specific surface area. However the curvature inherited from the templates restrict the exposure of {001} facets.

Mesocrystals are a new class of solid materials, which are built of crystallographically oriented nanocrystals.[16-18] Their unique structure may optimize the relationship between crystallite size and specific surface area.[17] Various $TiO_2$ mesocrystals have been synthesized.[19-25] Most of them are built of $TiO_2$ nanocrystals with rarely exposed {001} facets. Only a few methods have been developed to synthesize $TiO_2$ mesocrystals built of nanocrystals with largely exposed {001} facets.[23, 26-28] These hierarchically structured materials may not only optimize the relationship between crystallite size and specific surface area but also provide a large amount of highly active {001} facets. The known methods usually need corrosive HF, a high temperature hydrothermal reaction, a large amount of surfactant or other complex reaction conditions. These conditions restrain the potentialities of these materials for mass production and practical applications. An easier, greener, cheaper and more effective method is highly demanded.

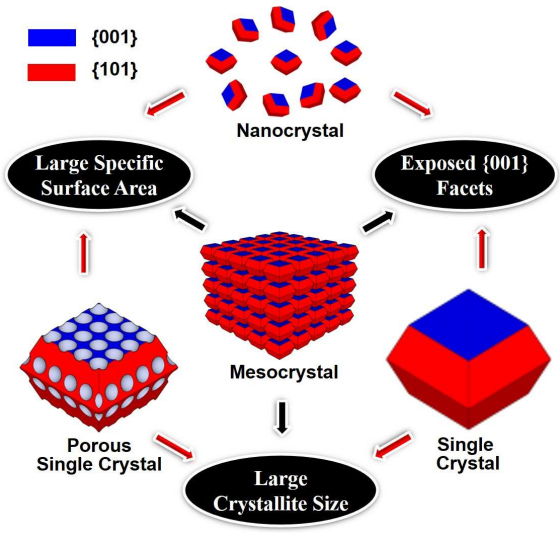


**Figure 1.** Relationship between common structure models of $TiO_2$ materials -- with largely exposed {001} facets and major factors that affect photocatalytic activity.

In this work, we creatively use the reaction between $NH_4OH$ and $(NH_4)_2TiF_6$ to prepare $NH_4TiOF_3$ mesocrystals and then converted them to $TiO_2$ mesocrystals *via* a topotactic transformation reaction.[20, 26] The experiment details are provided in ESI file.† For the preparation of the $NH_4TiOF_3$

mesocrystals, reaction solutions with different amounts of $(NH_4)_2TiF_6$ and $NH_4OH$ were tested. In some cases, the solutions became cloudy in the first half hour, suggesting precipitates formed. In other cases, the solutions kept clear without any evidence of precipitates even after 16 h. All precipitates were collected, cleaned and analyzed by Powder XRD. The results are summarized in Fig. 1a. When the concentrations of $(NH_4)_2TiF_6$ and $NH_4OH$ are equal or greater than 0.3 mol $dm^{-3}$ and 0.2 mol $dm^{-3}$ respectively, the main component of the final products is $NH_4TiOF_3$. Out of the range, ether nothing or poorly crystallized $TiO_2$ powders were obtained. A typical XRD pattern of the sample prepared in the solution with 0.4 mol $dm^{-3}$ $(NH_4)_2TiF_6$ and 0.3 mol $dm^{-3}$ $NH_4OH$ (denoted as $S_{43}$) is shown in Fig. 1b. All peaks are well matched with the PDF card of $NH_4TiOF_3$ (No. 54-0239), suggesting that the main component of the product is $NH_4TiOF_3$. The XRD patterns of other samples are given in ESI file (Fig. S1).

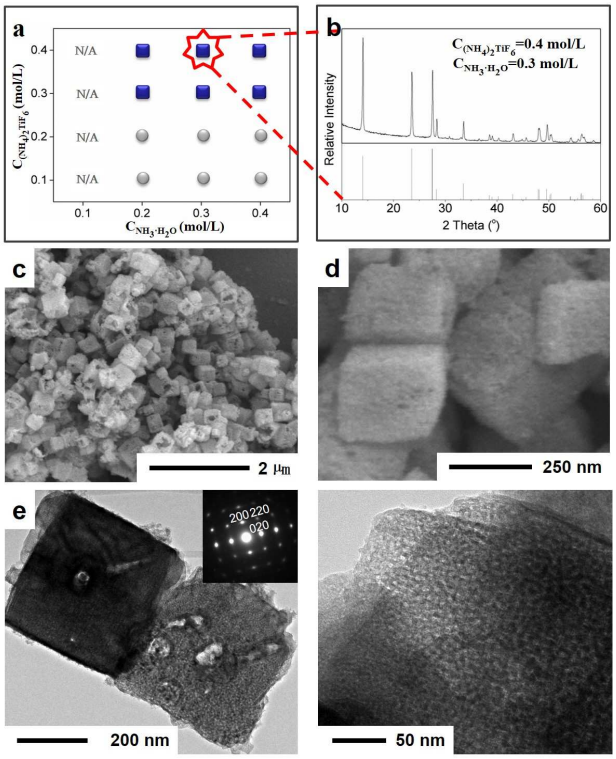


**Figure 2.** a) Summary of XRD results of the samples prepared in the solutions with different concentrations of $(NH_4)_2TiF_6$ and $NH_4OH$. A blue square means the main component of the products is $NH_4TiOF_3$. A grey circle means the main component of the products is a mixture of $NH_4TiOF_3$ and $TiO_2$. N/A means there are no precipitates in the solution after a certain reaction time. b), c), d), e) and f) XRD pattern, SEM images and TEM images of the sample prepared in the solution with 0.4 mol $dm^{-3}$ $(NH_4)_2TiF_6$ and 0.3 mol $dm^{-3}$ $NH_4OH$. Inset of e) is a SAED pattern.

SEM images of all as-prepared $NH_4TiOF_3$ samples are shown in Fig. S2. The results indicate that the morphology can be controlled by the ratio of $[(NH_4)_2TiF_6]/[NH_4OH]$. The SEM images of the sample $S_{43}$ is shown in Fig. 1c and 1d. The main products are cube-like particles with sizes of 200~500 nm. These particles are well separated without much aggregation, which is comparable with the particles prepared in presence of surfactants.[20, 26] The high resolution SEM image (Fig. 1d) indicates that these cube-like particles are not single crystals. There are many pores inside. The pores are clearly shown in the TEM images (Fig 1e and 1f). Pore sizes are about 5 nm. The SAED pattern (inset of Fig 1e) show "single-crystal-like" spot patterns with some distortion, typical for mesocrystals. The distortions come from small crystallographical mismatches between the nanocrystals (*i.e.* the building blocks).

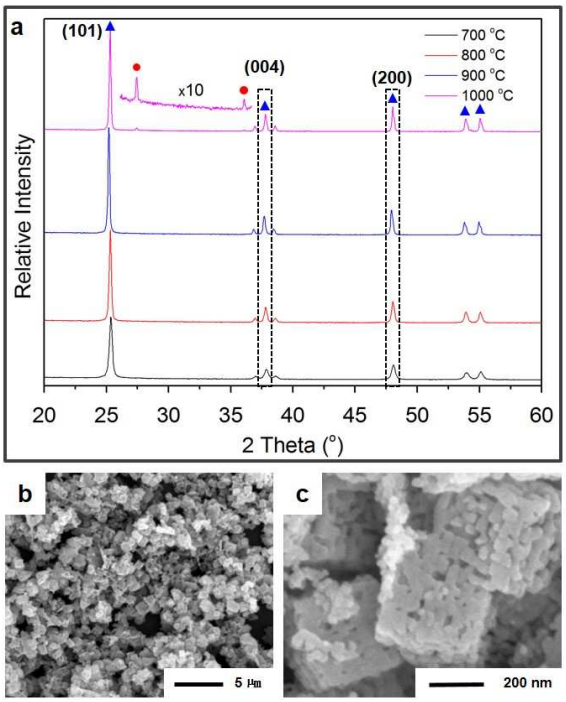


**Figure 3.** a) XRD patterns of the samples prepared by sintering the sample $S_{43}$ at different temperatures for 15 min. b) and c) low and high resolution SEM images of the sample $S_{43}$ sintered at 800 °C for 15 min.

In order to get $TiO_2$ mesocrystals, the as-prepared $NH_4TiOF_3$ samples have to be sintered at above 700 °C.[26] SEM images of all sintered samples are shown in Fig. S3. After sintering, all samples remained the overall shapes and sizes of the original samples. In order to examine the effect of sintering temperature on composition and morphologies. The sample $S_{43}$ were sintered at different temperature from 700 °C to 1000 °C. XRD patterns of all products are shown in Fig. 3a. The results indicate 700 °C is enough for $NH_4TiOF_3$ to convert to $TiO_2$. An interesting thing is that even being sintered at 1000 °C, only a very small part of particles transfer from anatase to rutile. The stability at high temperatures may be caused by stabilizing function of $F^-$ on the surface, which is consistent with others' work.[29, 30] The high temperature stability will increase their potentialities for practical applications. For these applications, a high temperature processing such as at up to 900 °C is necessary.[29]

SEM images of the sample sintered at 800 °C is shown in Fig 3b and 3c. It is obvious that the particles remain the overall shape and size after sintering. The higher resolution image (Fig 3c) indicates that the particles are built of nanoparticles with sizes of 20~30 nm and smooth surface. These nanoparticles are fused with each other at the edges, which leads to seldom finding an individual nanoparticles in the final products. SEM images of the samples sintered at other temperatures are shown in Fig. S4. When the sintering temperature is lower than 800 °C, the surface of nanoparticles are not smooth, suggesting the {001} facets are not completely exposed.[26] When the sintering

temperature is higher than 800 °C, with temperature increasing, the interspaces between nanoparticles disappear and therefore lead to smaller surface area.

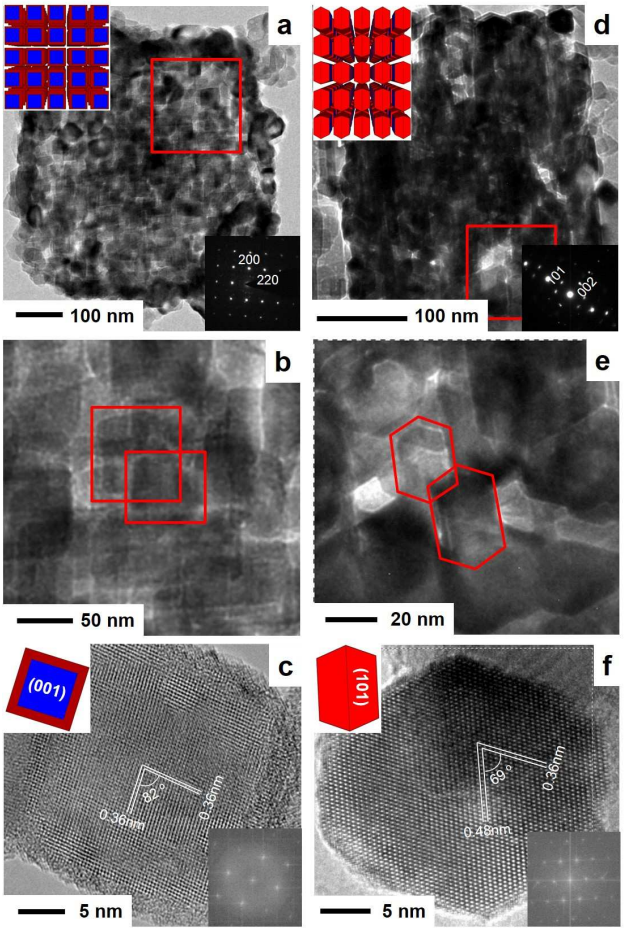


**Figure 4.** TEM images of the sample prepared by sintering the sample $S_{43}$ at 800 °C for 15 min. a), b) and c) viewed along the [001] direction. d), e) and f) viewed along the [010]/[100] direction.

The TEM images (Fig 4) give us more details about the building model of the sintered samples. Fig. 4a shows a sintered particle, which is built of nanoparticles. Most of the nanoparticles have sizes of 20~50 nm, square-like shape and fuse with each other (Fig. 4b). The SAED pattern (inset of Fig. 4a) show "single-crystal-like" diffraction with minor distortion. The distortions come from small mismatches between boundaries of the nanoparticles, which is typical for mesocrystals. The arrangement of the spots indicates that the particle is viewed along [001] direction of anatase $TiO_2$.[4] Fig. 4d shows another sintered particle, which is also built of nanoparticles. Most of these nanoparticles have hexagonal shape and similar orientation (Fig. 4e). The hexagon is a combine of two symmetrical trapezoids, which suggests that the particle is viewed along [100]/[010] direction of $TiO_2$.[4] The spot arrangement of the SAED pattern (inset of Fig. 4d) confirms our speculation. Based on the analysis of these two particles, it is unambiguous that the sintered particles are built of $TiO_2$ nanocrystals with exposed {001} facets. The schematic illustrations of the building model are given in the insets of Fig.4a and Fig. 4d.

The high resolution images of two nanoparticles with typical shapes are given in Fig. 4c and 4f, which give us more details of the subunit building block (*i.e.* the nanoparticles). The rhombus shape in Fig. 4c is observed through [11-1] zone axis. The (101) and (011) atomic planes with lattice spacing of 0.36 nm and 0.36 nm respectively are clearly shown. The (101) and (011) faces form the interfacial angle of 82 °C, which is very consistent with the theoretical value.[9] Fig. 4f shows a hexagon shape, suggesting it is viewed from to a pair of joint {101} facets. The (101) and (001) atomic planes with lattice spacing of 0.36 nm and 0.48 nm respectively are clearly shown. The (101) and (001) faces form the interfacial angle of 69 °C, which is very consistent with the theoretical value. Based on the analysis of HRTEM image, it is unambiguous that the $TiO_2$ nanoparticles are decahedron with dominant {001} facets. The schematic illustrations of the building blocks are given in the insets of Fig.4c and Fig. 4f.

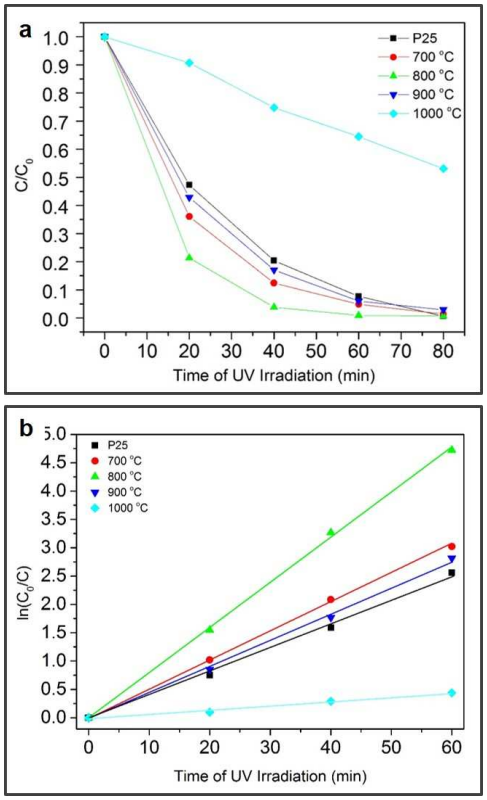


**Figure 5.** a) Photocatalytic activities of the samples prepared by sintering the sample $S_{43}$ at different temperatures for 15 min. b) Plots of $\ln C_0/C$ versus reaction time. $C_0$ is the initial concentration of methylene blue after being stirred in the dark for 1 h. C is the concentration of methylene blue after the reaction of time t.

Photocatalytic activities of the samples prepared by sintering the sample $S_{43}$ at different temperatures are shown in Fig. 5. It is clear that the 800 °C sample has the best performance. After 20 mins of UV irradiation, the decoloring ratio of methylene blue is close to 80% and much larger than that done by the commercialized P25 (50%). The degradation rate constant is almost twice as large as that of P25. In addition to the 800 °C sample, the photocatalytic activities of the 700 °C and 900 °C samples are also better than P25. Photocatalytic activity of a material is highly related with three factors, crystallite size, specific surface area and active facets. The specific surface area of the 800 °C sample is 25 $m^2$ $g^{-1}$, which is only half of that of P25 (56 $m^2$ $g^{-1}$). The good photocatalytic activity must not

come from a high specific surface area. The TEM results (Fig. 4) indicate that the 800 °C sample are built of $TiO_2$ nanocrystals with exposed {001} facets, which makes sure there are large amount of exposed {001} facets on the surface. The nanocrystals fused with each other along [010]/[100] direction, which leads to a relatively large crystallite size (~30 nm). The specific structure model of the 800 °C sample largely optimize the relationship among the three factors and therefore promote the photocatalytic activity. Lower or higher processing temperature such as 700 °C and 900 °C may damage the structure model (Fig. S4) and therefore deteriorate the photocatalytic activity.

## Conclusions

In this work, we developed a totally novel, extremely easy, much greener and low-cost method to prepare $TiO_2$ mesocrystals, which are built of nanoparticles with largely exposed {001} facets and superior photocatalytic ability. It need neither extremely toxic HF nor high-energy-consuming hydrothermal route. All you have to do is just to put $(NH_4)_2TiF_6$ and $NH_4OH$ into water and sinter the precipitates. This method is very robust and can be scaled up easily, which may pave the way for the mass production of anatase $TiO_2$ mesocrystals with exposed {001} facets. In addition to facile synthesis and superior photocatalytic ability, these particles have good photochemical stability (discuss is given in ESI file) and much larger size than P25, which make sure they can be easily removed from the system by filtering or centrifugation (Fig. S7 and S8) and reused. This increases their potentialities for practical applications. Another merit of the $TiO_2$ mesocrystals is that they can keep their superior photocatalytic ability even after being sintered at 900 °C. The high temperature stability is very important for some applications, such as ceramic tiles, asphalt and etc. For these applications, a high temperature processing procedure such as at up to 900 °C is necessary.

## Notes and references

[a] Department of Biomedical Engineering, School of Life Science and Technology, Huazhong University of Science and Technology, Wuhan, 430074, P. R. China.
E-mail: lei.zhou.public@gmail.com; Tel: +86-27-87792216
[b] Advanced Biomaterials and Tissue Engineering Center, Huazhong University of Science and Technology, Wuhan, 430074, P. R. China
† Electronic Supplementary Information (ESI) available. See DOI: 10.1039/c000000x/

## Acknowledgements

The work is supported by National Natural Science Foundation of China (NSFC, Grant No. 51172084 and 20901025).

## Reference

1 A. Fujishima, X. T. Zhang and D. A. Tryk, *Surf. Sci. Rep.*, 2008, **63**, 515.
2 F. Han, V. S. R. Kambala, M. Srinivasan, D. Rajarathnam and R. Naidu, *Appl. Catal. A*, 2009, **359**, 25.
3 K. Shankar, J. I. Basham, N. K. Allam, O. K. Varghese, G. K. Mor, X. J. Feng, M. Paulose, J. A. Seabold, K. S. Choi and C. A. Grimes. *The J. Phys. Chem. C*, 2009, **113**, 6327.
4 H. G. Yang, C. H. Sun, S. Z. Qiao, J. Zou, G. Liu, S. C. Smith, H. M. Cheng and G. Q. Lu, *Nature*, 2008, **453**, 638.
5 H. G. Yang, G. Liu, S. Z. Qiao, C. H. Sun, Y. G. Jin, S. C. Smith, J. Zou, H. M. Cheng and G. Q. M. Lu, *J. Am. Chem. Soc.*, 2009, **131**, 4078.
6 M. Liu, L. Piao, L. Zhao, S. Ju, Z. Yan, T. He, C. Zhou and W. Wang, *Chem. Commun.*, 2010, **46**, 1664.
7 J. Pan, G. Liu, G. Q. M. Lu and H. M. Cheng, *Angew. Chem. Int. Ed.*, 2011, **50**, 2133.
8 X. Han, Q. Kuang, M. Jin, Z. Xie and L. Zheng, *J. Am. Chem. Soc.*, 2009, **131**, 3152.
9 J. Zhu, S. Wang, Z. Bian, S. Xie, C. Cai, J. Wang, H. Yang and H. Li, *CrystEngComm*, 2010, **12**, 2219.
10 J. Yu, J. Fan and K. Lv, *Nanoscale*, 2010, **2**, 2144.
11 X. H. Yang, Z. Li, G. Liu, J. Xing, C. Sun, H. G. Yang, and C. Li, *CrystEngComm*, 2011, **13**, 1378.
12 T. R. Gordon, M. Cargnello, T. Paik, F. Mangolini, R. T. Weber, P. Fornasiero and C. B. Murray, *J. Am. Chem. Soc.*, 2012, **134**, 6751.
13 E. J. W. Crossland, N. Noel, V. Sivaram, T. Leijtens, J. A. Alexander-Webber and H. J. Snaith, *Nature*, 2013, **495**, 1.
14 W. Yue, X. Xu, J. T. S. Irvine, P. S. Attidekou, C. Liu, H. He, D. Zhao and W. Zhou, *Chem. Mater.*, 2009, **21**, 2540.
15 Z. Bian, J. Zhu, J. Wen, F. Cao, Y. Huo, X. Qian, Y. Cao, M. Shen, H. Li and Y. Lu, *Angew. Chem. Int. Ed.*, 2011, **50**, 1105.
16 H. Cölfen and M. Antonietti, *Angew. Chem. Int. Ed.*, 2005, **44**, 5576.
17 L. Zhou and P. O'Brien, *Small*, 2008, **4**, 1566.
18 R. Q. Song and H. Cölfen, *Adv. Mater.*, 2010, **22**, 1301.
19 L. Li and C. Liu, *CrystEngComm*, 2010, **12**, 2073.
20 L. Zhou, D. Smyth-Boyle and P. O' Brien, *J. Am. Chem. Soc.*, 2008, **130**, 1309.
21 P. Tartaj, *Chem. Commun.*, 2011, **47**, 256.
22 Z. Hong, M. Wei, T. Lan, L. Jiang and G. Cao, *Energy Environ. Sci.*, 2012, **5**, 5408.
23 Q. Chen, W. Ma, C. Chen, H. Ji and J. Zhao, *Chemistry*, 2012, **18**, 12584.
24 Z. Fang, L. Long, S. Hao, Y. Song, T. Qiang, and B. Geng, *CrystEngComm*, 2014, **16**, 2061.
25 R. O. Da Silva, R. H. Gonçalves, D. G. Stroppa, A. J. Ramirez and E. R. Leite, *Nanoscale*, 2011, **3**, 1910.
26 L. Zhou, J. Chen, C. Ji, L. Zhou, and P. O'Brien, *CrystEngComm*, 2013, **15**, 5012.
27 J. Feng, M. Yin, Z. Wang, S. Yan, L. Wan, Z. Li, and Z. Zou, *CrystEngComm*, 2010, **12**, 3425.
28 Z. Bian, T. Tachikawa, and T. Majima, *J. Phys. Chem. Lett.*, 2012, **3**, 1422.
29. S. C. Padmanabhan, S. C. Pillai, J. Colreavy, S. Balakrishnan, D. E. McCormack, T. S. Perova, S. J. Hinder and J. M. Kelly, *Chem. Mater.*, 2007, **19**, 4474.
30. K. Lv, J. Yu, L. Cui, S. Chen, and M. Li, *J. Alloys Compd.*, 2011, **509**, 4557.



 